



GLOBAL JOURNAL OF RESEARCHES IN ENGINEERING
MECHANICAL AND MECHANICS ENGINEERING
Volume 11 Issue 7 Version 1.0 December 2011
Type: Double Blind Peer Reviewed International Research Journal
Publisher: Global Journals Inc. (USA)
Online ISSN: 2249-4596 Print ISSN:0975-5861

Neurofuzzy Implementation in Smart Toolpost to Improve Performance

By Maki K. Rashid

Mechanical and Industrial Engineering Sultan Qaboos University.

Abstract - Machining is a complex process that requires a high degree of precision with tight geometrical tolerance and surface finish. Those are confronted by the existence of vibration in the turning machine tool. Overcoming a micro level vibration of a cutting tool using smart materials can save old machines and enhance flexibility in designing new generations of machine tools. Using smart materials to resolve such problems represent one of the challenges in this area. In this work the transient solution for tool tip displacement, the pulse width modulation (PWM) technique is implemented for smart material activation to compensate for the radial disturbing cutting forces. A Neurofuzzy algorithm is developed to control the actuator voltage level to improve dynamic performance. The deployment of the finite element method in this work as a dynamic model is to investigate the ability of the in intelligent techniques in improving cutting tool accuracies. The influence of minimum number of PWM cycles with each disturbing force cycle is investigated in controlling the tool error growth. Toolpost structural force excitation due to the PWM cycles was not given adequate attention in previous publications. A methodology is developed to utilize toolpost static force-displacement diagram to obtain required activation voltage to shrink error under different dynamic operating conditions using neurofuzzy.

Keywords : *Tool vibration, Smart Material, Vibration suppression, Cutting tool, Neurofuzzy*

GJRE-A Classification: *FOR Code: 091304*



NEUROFUZZY IMPLEMENTATION IN SMART TOOLPOST TO IMPROVE PERFORMANCE

Strictly as per the compliance and regulations of:



© 2011 Maki K. Rashid. This is a research/review paper, distributed under the terms of the Creative Commons Attribution-Noncommercial 3.0 Unported License <http://creativecommons.org/licenses/by-nc/3.0/>), permitting all non commercial use, distribution, and reproduction in any medium, provided the original work is properly cited.

Neurofuzzy Implementation in Smart Toolpost to Improve Performance

Maki K. Rashid

Abstract - Machining is a complex process that requires a high degree of precision with tight geometrical tolerance and surface finish. Those are confronted by the existence of vibration in the turning machine tool. Overcoming a micro level vibration of a cutting tool using smart materials can save old machines and enhance flexibility in designing new generations of machine tools. Using smart materials to resolve such problems represent one of the challenges in this area. In this work the transient solution for tool tip displacement, the pulse width modulation (PWM) technique is implemented for smart material activation to compensate for the radial disturbing cutting forces. A Neurofuzzy algorithm is developed to control the actuator voltage level to improve dynamic performance. The deployment of the finite element method in this work as a dynamic model is to investigate the ability of the intelligent techniques in improving cutting tool accuracies. The influence of minimum number of PWM cycles with each disturbing force cycle is investigated in controlling the tool error growth. Toolpost structural force excitation due to the PWM cycles was not given adequate attention in previous publications. A methodology is developed to utilize toolpost static force-displacement diagram to obtain required activation voltage to shrink error under different dynamic operating conditions using neurofuzzy.

Keywords : *Tool vibration, Smart Material, Vibration suppression, Cutting tool, Neurofuzzy*

I. INTRODUCTION

Improving quality of surface finish and geometrical accuracies during machining using active material was under intensive investigation (Park, et al. 2007). Raw material conversion to new product requires material removal processes using machine tool. Demand for higher productivity in automated manufacturing brought attention for controlling machine tool dynamics for better machining accuracy. Both economic and ecological factors encouraged old conventional machines to continue in service by overcoming tool vibration problems. Various factors might affect the machining process, some of them are non-measurable and others might change in real-time. However, the wider use and the availability of cost effective microcontrollers encouraged the implementation of intelligent control schemes to overcome such time dependent machining problems (Krzysztof, et al. 2011). The tiny unfavorable relative

motion between the cutting tool and the working piece that associated with high excitation forces encouraged the use of smart material actuators to counteract such motion errors (Radecki, et al. 2010). The rigid fixture is a good choice for minimizing displacements of cutting tools from its nominal position during machining. Unfortunately, such option is not available in all applications. The reconfigurable manufacturing era prefers fixtures consumes less space with minimum weight (Gopalakrishnan, et al. 2002; Moon and Kota 2002).

When the control system, and real time microprocessor implementation were examined no details were given for the design and selection of actuator, tool holder, and tool bit stiffness, and, actuator switching. Also in the case of future geometrical changes, the validity of using lumped masses in system modeling is questionable. Information is required regarding the nature and type of signals controlling smart material and how might affect toolpost dynamic response. Recently a tool adaptor is used with built-in active vibration damping device to dynamically stabilize the turning process (Harms, et al. 2004). The vibration compensation system is based on a multilayer piezo-actuator in collocation with a piezoelectric force sensor. An analogue controller based on integral force feedback method is used for active damping. Latest dynamic modeling of smart toolpost (Rashid, 2005) is based on continuous elastic structural toolpost overcoming previous limitations of lumped mass modeling without further steps toward the development of a generalized scheme for tool error attenuation. Such models are then implemented for designing an adaptive controller using fuzzy controller (Rashid, 2006).

This work is implementing the finite element method (FEM) to model flexible smart tool post incorporating PZT actuator, tool holder, supporting fixture, and tool bit, and, discusses the effect of structural properties on the critical frequencies as compared to lumped mass modeling. Also investigate the effectiveness of the developed Neurofuzzy algorithm in controlling error attenuation under different excitation cutting force frequencies. The tool radial motion that causes dimensional variation in the work-piece is emphasized. The smart toolpost static force-displacement analysis under different voltage input is integrated with the development the Neurofuzzy scheme

Author : *Mechanical and Industrial Engineering Sultan Qaboos University. P. O. Box: 33 Al-Khod Postal Code No.123 Muscat, Sultanate of Oman. E-mail : maki@squ.edu.om*

to predict the activation voltage in dynamic error attenuation. A special attention is given for the model to be a robust for large variations in design parameters. Such a finite element model offers a methodology for micro-vibration attenuation in smart toolpost using smart materials and intelligent schemes like Neurofuzzy.

II. THE TOOLPOST FEM MODEL

In this work Lead Zirconate Titanate (PZT), is employed as a smart material actuator. This is encouraged by a well-developed theoretical analysis of this material. Also it is the most common used piezoelectric materials. The Toolpost model incorporates actuator, tool carrier (holder), supporting diaphragm, and tool bit (spring buffer between the tool carrier and the net actuating force at tool tip) as shown in Figure 1.

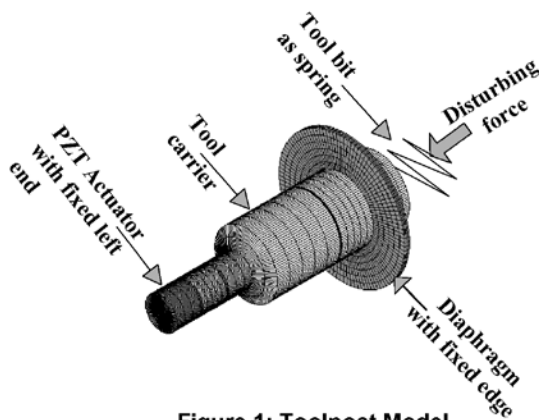


Figure 1: Toolpost Model

a) Model Governing Equations

The model consists of a conventional stacked PZT actuator contains polarized ferroelectric ceramic in the direction of actuation,

$$\{T\} = [c^E] \{S\} - [e]^T \{E\} \tag{1}$$

$$\{D\} = [e] \{S\} + [\epsilon^S] \{E\}$$

adhesive, supporting structure, and electrically wired electrodes as shown in Figure 2.

The finite element modeling of the PZT actuator and toolpost is developed (Piefort 2001) by using the general constitutive equations of linear piezoelectricity and equations of mechanical and electrical balance.

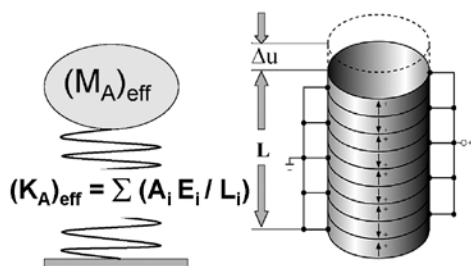


Figure 2: PZT Stacked Actuator

The momentum balance equation is

$$\rho \{\ddot{u}\} = \nabla \cdot \{T\} \tag{2}$$

And the electric balance equation is

$$\nabla \cdot \{D\} = 0 \tag{3}$$

Knowing, $\{S\} = \nabla^S \cdot \{u\}$, $\{E\} = -\nabla \phi$

Where $\{T\}$ represents the stress vector, $\{S\}$, the strain vector, $\{E\}$, the electric field, $\{D\}$, the electric displacement, $[c^E]$, the elastic coefficients at constant $\{E\}$, $[\epsilon^S]$, the dielectric coefficients at constant $\{S\}$, and $[e]$, the piezoelectric coupling coefficients. As well $\{u\}$ is the mechanical displacement vector and $\{\ddot{u}\} = \partial^2 \{u\} / \partial t^2$ is the acceleration. In addition ϕ is the electric potential (voltage). The boundary conditions are shown in Figure 1, as represented by the fixed end conditions for both, actuator left side and, diaphragm outer edge. The model description is completed by specifying the applied voltage at actuator electrodes' using the PWM technique weighted by a factor worked out from the developed fuzzy algorithm and based on the inputs from the calculated toolpost dynamic response.

b) Building The Finite Element Equations

The finite element model of this work is built by using the piecewise application of classical variational methods on smaller and simpler sub-domains connected to each other by a finite number of nodes. A 8-node isoparametric solid element is used for domain discretization. The unknowns are the displacements vector u_i and the electric potential values ϕ_i at node i. The formulation of the dynamic equations of a piezoelectric continuum is discussed thoroughly in the literature (Allik and Hughes 1970; Lerch 1990). Taking into account the constitutive equations (1) and by introducing the Lagrangian and virtual work formulation into the Hamilton's principle we that satisfies the arbitrary deviation of the displacements $\{u_i\}$ and the electrical potentials $\{\phi_i\}$ and their compatibilities with the compatibilities with the associated boundary conditions,

$$[m_{uu}] \{\ddot{u}_i\} + [c_{uu}] \{\dot{u}_i\} + [k_{uu}] \{u_i\} + [k_{u\phi}] \{\phi_i\} = \{f_i\} \tag{4}$$

$$[k_{u\phi}]^T \{u_i\} + [k_{\phi\phi}] \{\phi_i\} = \{q_i\}$$

$[m_{uu}]$, $[k_{uu}]$ and, $[c_{uu}]$ are the mechanical mass, stiffness, and, $[k_{\phi\phi}]$ damping matrices, respectively. $[k_{u\phi}]$ is the piezoelectric coupling matrix and, $[k_{\phi\phi}]$ is the dielectric stiffness matrix. $\{f_i\}$ and $\{q_i\}$ are the nodal mechanical force and electric charge vectors, respectively. and, are the nodal displacement and potential vectors, respectively. For the sake of brevity,

the scheme by which the elemental contributions are assembled to form the global system matrices are discussed in (Zienkiewicz and, Taylor 2000a, b).

III. NATURAL FREQUENCY COMPARISON BETWEEN LUMPED AND FEM MODELING

The lumped mass modeling of the PZT actuator and tool carrier generate a simple closed form solution that is of interest to designers and modelers. However using such model in different applications requires more alertness. Most applications require a precise displacement sensing and accurate prediction for natural frequency to ensure the effective control for smart material actuator.

a) Comparative Results for PZT Actuator

Mode shapes and the resonant frequencies for undamped system are obtained by using Eigenvalue analysis. Free vibration implies that $\{f_i\} = 0$ and $\{q_i\} = 0$ in equation (4). Modal analysis is based on the orthogonality principle of natural modes and expansion theorem (Zienkiewicz and Taylor 2000 b).

The fundamental angular undamped natural frequency of a beam of fixed –free end condition is represented by:

$$\omega_n = \frac{\pi}{2L} \sqrt{\frac{E}{\rho}} \tag{5}$$

Usually the actuator is composed of several PZT layers, electrodes, adhesive, and supporting structure as shown in Figure 2. To compare between simple calculations and the FEM solutions the actuator effective stiffness assumed to be the stiffness sum in the series for all individual layers neglecting all piezoelectric effects.

$$KA = \sum \left(\frac{A_i E_i}{L_i} \right) \tag{6}$$

Actuator effective lumped mass is estimated to be a 20 or 30% of the summed layers masses as indicated in Figure 3.

$$(M_A)_{eff} = (0.2 \text{ or } 0.3) \sum (A_i \rho_i L_i) \tag{7}$$

$$\omega_{Lumped} = \sqrt{\frac{K_A}{(M_A)_{eff}}} \tag{8}$$

Then,

The FEM solutions for the actuator first natural frequency under short circuit (zero piezo effect) and open circuit conditions (maximum piezo effect) compare to the estimated lumped mass natural frequency as given in Eq. (8) and their ratios plotted in Figure 3. Present calculations are based on PZT8 property from (Berlincourt and Krueger 2000).

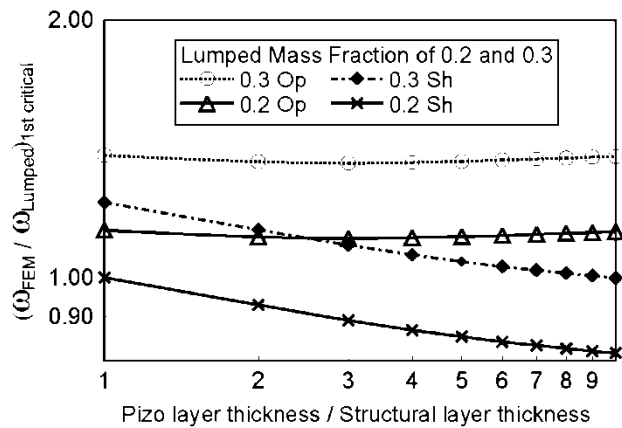


Figure 3: First critical frequency ratio (FEM / Lumped) versus layers thickness ratios for short circuit (Sh) and open circuit (Op)

Plotted results in Figure 3 neglected any stiffness variation that might result from actuator fabrication. The short circuit actuator (Sh) gave lower value for natural frequency indicating a lower stiffness in the absence of piezo effect. Such data is offering the designers a rapid tool for estimating natural frequencies in the early stages of design. The short (Sh) and open circuit (Op) conditions map the extremes of natural frequency values. The deviation in natural frequencies between the FEM and lumped mass solutions are different between open and short circuit conditions.

b) Comparative Results for Integrated Toolpost

Incorporating the tool carrier and the supporting diaphragm to the PZT actuator model introduces the multi-degree of freedom system. In this work the effective mass at the actuator end $(M_{AE})_{eff}$ in Fig. 4 represent 30% of the combined actuator and tool carrier masses. While the effective mass near to the diaphragm end $(M_{CE})_{eff}$ is 30% of the combined tool carrier and diaphragm masses. Higher mass percentages resulted in a higher deviation from the FEM solutions. Solutions for the two-degree of freedom system incorporating piezoelectric coupling effects are investigated by (Frankpitt 1995; Abboud, et al. 1998). However, the significant deviation between the FEM and the lumped mass solution and its range of applicability has not investigated. KA is calculated as in Eq. (6) which is shown in Fig. 4 as a coupling stiffness joining $(M_{AE})_{eff}$ and the ground. The tool carrier stiffness KC is calculated accordingly from the relation $(A_C E_C / L_C)$. The tool carrier stiffness KC is calculated accordingly from the relation $(A_C E_C / L_C)$.

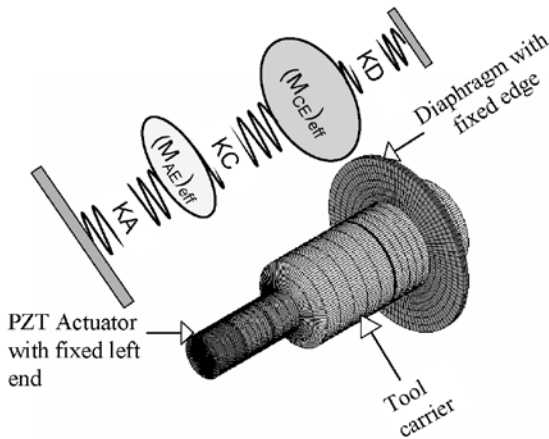


Figure 4: Tool Carrier and Actuator with Diaphragm

Diaphragm stiffness (KD) is based on plate theory with fixed central hole at both inner and outer edges, (Roark and Young 1975). Then the stiffness matrix of this 2-degree of freedom system shown in Figure 4 is:

$$[K] = \begin{bmatrix} KA + KC & -KC \\ -KC & KC + KD \end{bmatrix} \quad (9)$$

Modal shapes and frequencies that resulted from the FEM model compare to the lumped mass model in Figure 4 by considering three different frequency ratios, namely $(\omega_{FEM})_{1st} / (\omega_{Lumped})_{1st}$ for 1st critical, $(\omega_{FEM})_{2nd} / (\omega_{Lumped})_{2nd}$ for 2nd critical, $(\omega_{FEM})_{3rd} / (\omega_{Lumped})_{2nd}$ and for 3rd critical. Structural stiffness contributions to these frequency ratios are presented in Figures 5-7 including tool carrier to actuator stiffness (KC/KA) and diaphragm to actuator stiffness (KD/KA) under both open and closed circuit conditions.

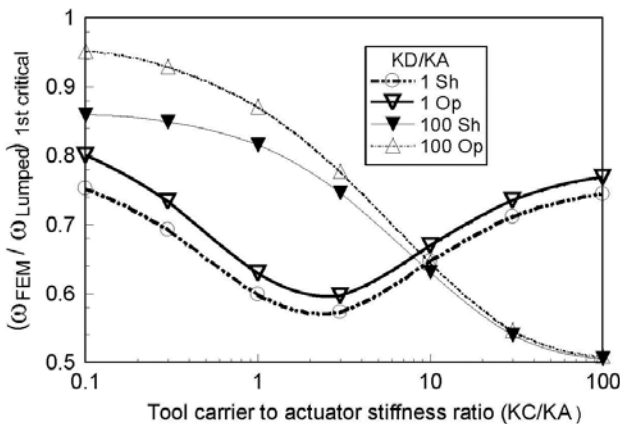


Fig. 5: First critical frequency ratio of FEM to lumped mass solutions versus (KC/KA) at different (KD/KA) for open (Op) and short (Sh) circuits

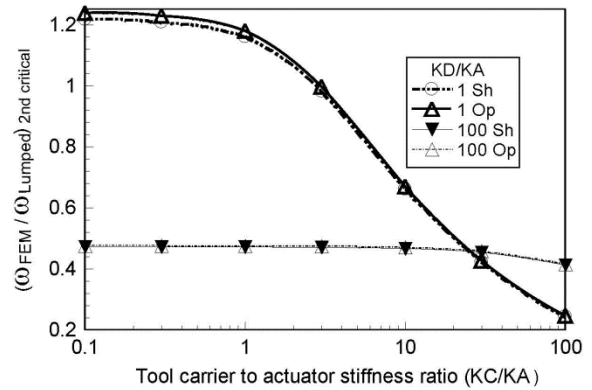


Fig. 6 Second critical frequency ratio of FEM to lumped mass solutions versus (KC/KA) at different (KD/KA) for open (Op) and short (Sh) circuits

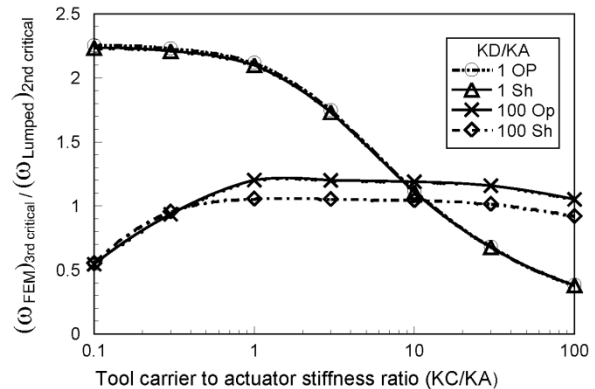


Fig. 7: Ratio of FEM third critical to second lumped mass critical frequency versus (KC/KA) at different (KD/KA) for open (Op) and short (Sh) circuits

Figure 5 indicates significant dependence of $(\omega_{FEM})_{1st} / (\omega_{Lumped})_{1st}$ for 1st critical with the variations in tool carrier to actuator stiffness (KC/KA) and diaphragm to actuator stiffness ratio (KD/KA). The availability of such results would help to work out a lumped mass model that has a more realistic response based on problem assumptions. The difference between first critical frequency ratios for short (sh) and open (Op) circuit conditions diminish at high (KC/KA) especially when (KD/KA) is relatively high.

The second critical frequency ratio $(\omega_{FEM})_{2nd} / (\omega_{Lumped})_{2nd}$ on the semi-log plot of Figure 6 shows independency of such ratio on tool carrier stiffness when selecting higher ratio of (KD/KA) which is not recommended for actuator design. At low (KD/KA) the dependency of frequency ratio on (KC/KA) is much more distinguished. In general the frequency ratio is tending to change remarkably when (KC/KA) goes beyond ten.

Ratio of the FEM third critical frequency $(\omega_{FEM})_{3rd}$ to the second critical frequency $(\omega_{Lumped})_{2nd}$ of lumped model shown in Figure 7 have a similar trend

as in Figure 6. The considerable difference between open and short circuit conditions occurs at high (KD/KA) only. Results indicate a possibility for $(\omega_{FEM})_{3rd}$ to be lower than $(\omega_{Lumped})_{2nd}$. Such disagreement between lumped mass models and FEM solution requires more awareness in vibration controller design using smart materials.

IV. TOOLPOST FORCE GENERATION VERSUS DISPLACEMENT

Effective tool error attenuation depends on PZT actuator capabilities for resisting tool axial force within the required limited range of motion. To obtain such data a force versus displacement curve is developed for the investigated toolpost in Figure 1. Figure 8 shows the force-displacement characteristics for different values of tool carrier to actuator stiffness ratio (KC/KA). The plotted curves in Figure 8 are emphasizing the importance of increasing (KC/KA). Similar plots are generated to obtain the effects of increasing (KT/KA) and (KT/KA). Resulted figures indicate the worth of reducing the structural support stiffness (diaphragm) in the direction of PZT activation to improve actuation force for error attenuation. Guessing first actuator design can be conducted according to information offered by force-displacement calculations. A special treatment for dynamic effects during machining is discussed in the next sections. The smart material data and, the investigated toolpost dimensions that applied to both static and dynamic calculations are given in Table 1. A general theory for a piezoelectric actuator subjected to mechanical excitations and feedback voltages is discussed in (Tzou 1991).

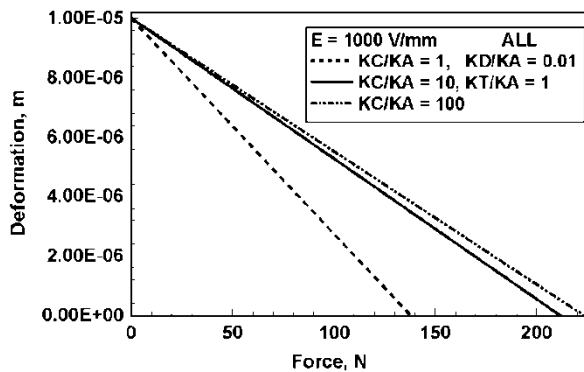


Figure 8: Smart toolpost displacement versus the applied force for different tool carrier to actuator stiffness ratio.

Table 1 : Toolpost dimension and material

Item	Value	Units
Cylindrical PZT-8 Stack		
PZT Thickness	0.09e-03	m
Electrode Thickness	0.03e-03	m
Structural support	0.03e-03	m
Adhesive Thickness	10.0e-06	m
Number of layers	500	
Effective Radius	5.0e-3	m
Steel Cylindrical Tool Carrier (holder)		
Radius	10.0e-3	m
Length	55.0e-3	m
Steel Tool Bit Effective Length		
Assumed Effective Length	20.0e-3	m
Steel Diaphragm		
Thickness	0.5e-3	m
Outside Radius	20.0e-3	m

V. NEUROFUZZY ALGORITHM FOR VOLTAGE ACTIVATION

Obtained results from Figures 5-7 prove significant deviation of lumped mass modeling from the finite element solution of the continuous elastic structure especially in the range of low (KD/KA) and high (KC/KA) where the PZT actuation is maximum as pointed out in Figure 8. Therefore the finite element method is the only reliable and available tool of solution in assessing switching methodology and system damping in the smart toolpost toward effective error reduction. Transient solution for tool displacement is achieved by solving Eq. (4) in the time domain for the system shown in Figure 1. The smart toolpost configuration and its associated data are given in Table 1.

a) PWM Modeling

The possibility of reducing tool tip position error is conducted by appropriate voltage activation to the smart material. Using Pulse Width Modulation (PWM) is an economical implement for smart material activation for such application. It is a common technique used with microcontroller units (MCU) to govern the time average of power input to the actuators. The associated time dependent motion accompanying tool vibration during error reduction is our next concern.

The voltage activation to the smart material is either triggered by a piezo stack with force sensing layer or by using a suitable type of displacement sensor. In both methods sensing the location should reflect cutting tool position error correctly. Switching circuits design is not discussed in this work; however the required voltage intensity level and the resulted motion are emphasized in this work.

Setting up the switching voltage by a series of PWM cycles should be judged by a sensed cutting force value from the peak force spectrum at the peak force

frequency (ω_f), then, the initial peak voltage is estimated from Figure 8. A complete period of the peak force cycle (T_f) is divided into number of duty cycles (N_{PWM} or NPWM). Then, for any of these divisions, the time duration of the PWM high DC-voltage is calculated based on the obtained voltage factor from the neurofuzzy algorithm that will be discussed next. A time delay in voltage activation can be incorporated as a function of the peak force frequency period. Two switching's are associated with each PWM cycle segment, therefore switching rate is $2N_{PWM}\omega_f$. Effects of switching voltage input, forcing frequency ω_f , and, damping level upon toolpost time response are parameters to be discussed in a smart toolpost transient solution.

b) *Controller Configuration*

It is difficult to acquire a controller that ensures continuous error tracking under stabilized condition for smart toolpost under continuous exposal to an erratic real time force inputs. The use of intelligent controller is generated by the random nature of system excitations which largely depends on unpredictable parameters such as structural properties, friction, and other variable dynamic forces. A neural network can model the response of such system by means of a nonlinear regression in the discrete time domain. The result is a network, with adjustable weights, that might approximate the system dynamics. Though it is a problem since the knowledge is stored in an opaque fashion and the learning results in a large set of parameter values which almost impossible to be interpreted in words. Conversely using a fuzzy rule based controller that consists of readable if-then statements which is almost a natural language, cannot learn new rules alone. The neurofuzzy controller might be preferred over the others for such application since it combines the two and it has a learning architecture (Lin, J. and Chao, W.S., 2009). To construct a neurofuzzy controller with ANFIS (Adaptive Neuro Fuzzy Inference System), we need a set of input-output data. In this work, two input signals are considered. The first input is normalized error defined by representing the negative error by the tool tip displacement away from the work piece axis. Then is the negative of the normalized tool tip error with respect to the maximum static displacement of the peak radial cutting force? The universe of discourse of the input variable is defined to be within the range [0, 1]. The second input is the normalized rate of change in error. Basically represent the time rate of change of error calculated every one tenth of the force period and given a universe of discourse [-0.2, 0.2]. The output signal is VF a multiplication factor for the estimated voltage from the static tool force-displacement chart in Figures 9 and 10 and given a universe of discourse [0, 1].

Control strategies under different design parameters that might be difficult to implement in a real experimental setup can be tested by using the finite element dynamic simulation with ordinary Sugeno's Fuzzy controller. All problem components are integrated through visual basic as shown in Figures 9 and 10. Data sets are collected for training and adapting the Neurofuzzy controller in the next stage. The cost effectiveness of such simulation definitely adds to its flexibility in exploring different dynamic parameters that might be difficult to introduce in actually built system.

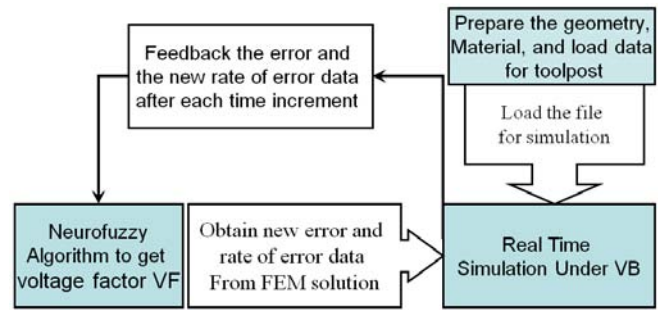


Fig. 9 Simulation flow chart

c) *Takagi-Sugeno model*

The general Takagi-Sugeno rule structure is:

If $g(e_1 \text{ is } A_1, e_2 \text{ is } A_2, \dots, e_k \text{ is } A_k)$ then

$$y = f(e_1, e_2, \dots, e_k) \quad (10)$$

Here f is the logical function which connects the sentences that form the implemented conditions, y is the output, and, f is a function of the inputs e_1, e_2, \dots , and e_k . The inputs in this work are the normalized error ϵ and the normalized rate of change in error $\dot{\epsilon}$, while the output is the voltage factor VF.

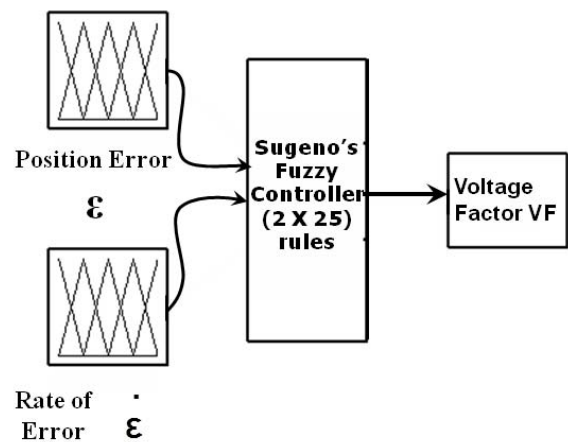


Fig. 10. Sugeno's Controller Layout

The rules can be structured according to the importance of the actual parameters involved in the targeted application based on the simulated dynamic model. The Takagi and Sugeno's fuzzy model can be formulated as the following:

$$L^i: \text{ IF } e_1 \text{ is } A_1^i \text{ and } \dots \text{ and } e_k \text{ is } A_k^i \text{ THEN } y^i = f_i = a_0^i + a_1^i \cdot e_1 + \dots + a_k^i \cdot e_k \quad (11)$$

where, $L^i (i = 1, 2, \dots, n)$ denotes the i -th rule, n is the number of fuzzy rules, y^i or f_i is the output from the i -th rule (implication), $a_p^i (p = 0, 1, \dots, k)$ are consequent parameters, e_1, e_2, \dots, e_k are the input variables, and A_p^i are fuzzy sets whose membership functions are denoted by the same symbols as the fuzzy values. Given an inputs (e_1, e_2, \dots, e_k) the final output of the fuzzy model is inferred by taking the weighted average of the f_i is:

$$y = \frac{\sum_{i=1}^n w_i f_i}{\sum_{i=1}^n w_i} \quad (12)$$

where $w_i > 0$ and f_i is calculated for the input by consequent equation of the i -th rule, and the weight w_i implies the overall truth value of premise of the i -th rule for input calculated as

$$w_i = \prod_{p=1}^k A_p^i \cdot e_p \quad (13)$$

d) *The Neuro-fuzzy control algorithm*

To facilitate the learning (or adaptation) of the Takagi-Sugeno fuzzy model, it is convenient to implement the fuzzy model into a framework of adaptive network that can compute gradient vectors systematically. The resultant network architecture called ANFIS (Adaptive Neuro-Fuzzy Inference System). ANFIS is described by a similar Takagi-Sugeno model with a single difference that in this case the inputs, e_1 (ϵ - Error) and, e_2 ($\dot{\epsilon}$ - Rate of Error) are range values. The fuzzy set for ϵ being $A_1 = \{ L = \text{“Low”}, M/L = \text{“Medium to low”}, M = \text{“Medium”}, M/H = \text{“Medium to High”} \text{ and } H = \text{“High”} \}$, and fuzzy set for $\dot{\epsilon}$ being $A_2 = \{ L = \text{“Low”}, M/L = \text{“Medium to low”}, M = \text{“Medium”}, M/H = \text{“Medium to High”} \text{ and } H = \text{“High”} \}$. Fig. 11 illustrate graphically the neurofuzzy reasoning mechanism to derive an output y from a given inputs ϵ and $\dot{\epsilon}$. Output f_i is one of the voltage factor VF for i -th rule where the size of the rule base is 25. The dynamic simulation is conducted with several types and sizes of membership functions for the fuzzy sets A_1 and, A_2 . The triangular membership functions and a size of five for each of the two fuzzy sets were found the simplest and best suited for this case.

The square elements in Fig. 11 represent the adaptive nodes depending on the parameter set of the adaptive network. The circles represent fixed nodes, which are independent of the parameter set. The first

layer is composed of adaptive nodes representing the triangular membership functions (Jang, J.-S. R.; Sun, C.-T. & Mizutani, E. 1996) associated with each linguistic value. The second layer implements the fuzzy rules. Each node in this layer calculates the firing strength of a rule by means of multiplication between the membership degrees of the two inputs. The third layer consists of adaptive nodes which include the output membership.

The other two layers consist of fixed nodes that implement the weighted average procedure to obtain the voltage factor VF as shown in Fig. 11. As the size of the rule base of the Sugeno fuzzy inference system (SFIS) is 25, we will have to identify 75 consequent parameters $\{ a_0^1, \dots, a_0^{25}, a_1^1, \dots, a_1^{25}, a_2^1, \dots, a_2^{25} \}$ as indicated in Jang, J.-S. R.; Sun, C.-T. & Mizutani, E. (1996). This can be obtained from the neural network (NN) using training set $\{ \epsilon, \dot{\epsilon}, VF \}$ which are collected from the dynamic simulation results by using the Sugeno fuzzy inference system. A back-propagation learning algorithm is used to identify these parameters in two steps. In the forward pass, the input membership functions are fixed and consequent parameters associated with the output are calculated by applying the least square estimation method. Using these parameters, the NN generates an estimate of the output voltage factor VF. The difference between this estimate and the motor's value from the training set is then back-propagated in a second pass when the premise parameters associated with the input membership functions are calculated

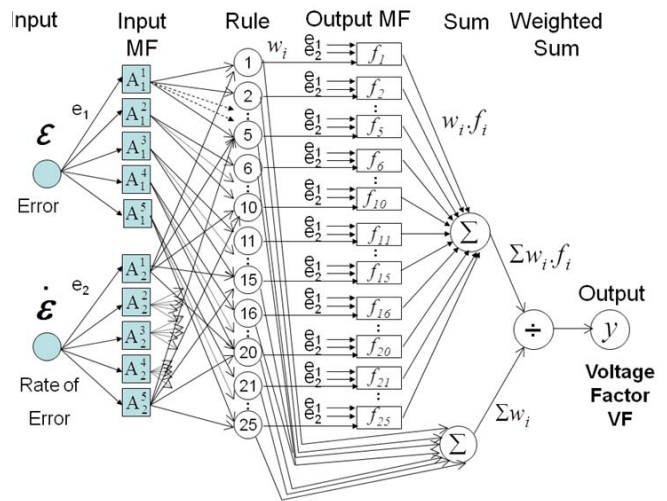


Fig.11 ANFIS architecture

e) *Solution Method for Dynamic Equations*

The system of equations for such a nonlinear problem is best solved by classical Newmark algorithms (Abboud, et al. 1998). Time step-by-step integration is used in solving Eq. (4). Basically the final results are obtained by attaining the solution at present time step from known solution at the previous time step. This approach takes into consideration the higher order time

approximations. Also it assumes a constant acceleration over a small time interval (time-step). By considering the Taylor series quadratic expansion for the function $\{u\}$ and its derivatives, (Abboud, et al. 1998) then,

$$\left. \begin{aligned} \{u_i\}_{n+1} &= \{u_i\}_n + \Delta t \{\dot{u}_i\}_n + \frac{1}{2}(1 - \beta_2)\Delta t^2 \{\ddot{u}_i\}_n + \\ &\frac{1}{2}\beta_2\Delta t^2 \{\ddot{u}_i\}_{n+1} = \{\dot{u}_i\}_{n+1} + \frac{1}{2}\beta_2\Delta t^2 \{\ddot{u}_i\}_{n+1} \\ \{\dot{u}_i\}_{n+1} &= \{\dot{u}_i\}_n + (1 - \beta_1)\Delta t \{\ddot{u}_i\}_n + \beta_1\Delta t \{\ddot{u}_i\}_{n+1} \\ &= \{\ddot{u}_i\}_{n+1} + \beta_1\Delta t \{\ddot{u}_i\}_{n+1} \end{aligned} \right\} (14)$$

From the dynamic equation Eq. (5) we have

$$[m_{uu}]\{\ddot{u}_i\}_{n+1} + [c_{uu}]\{\dot{u}_i\}_{n+1} + [k_{uu}]\{u_i\}_{n+1} + [k_{u\phi}]\{\phi_i\}_{n+1} = \{f_i\}_{n+1} \quad (15)$$

Equations (14) and (15) allows three unknowns $\{u_i\}_{n+1}$, $\{\dot{u}_i\}_{n+1}$ and, $\{\ddot{u}_i\}_{n+1}$ to be determined and for brevity the detail of solving these equations and the values of β_1 and, β_2 are given in (Abboud, et al. 1998). The step-by-step integration scheme assumes a known structural damping. The damping matrix is assumed to be a linear combination of stiffness and mass matrices (Rayleigh damping) (Bathe 1982):

$$[c_{uu}] = \alpha[m_{uu}] + \beta[k_{uu}] \quad (16)$$

Where α and β are constants to be determined from two assumed modal damping ratios (ξ_i) (1% and 5%) for first and second natural frequencies respectively which are related to modal damping by the available established relations.

VI. RESULTS OF FUZZY CONTROLLED RESPONSE FOR INTEGRATED TOOLPOST

Requirements to reduce tool holder size and weight encourage developing new tactics of using smart actuators to attain high precision by compensating unfavorable motion errors. Estimation of cutting tool radial force might involve several variables. In general the static force relation (Frankpitt 1995) which expressed in terms of depth of cut (d , mm), cutting speed (V , mm/s), feed rate (f , m m/rev), and, coefficients describing the nonlinear relationships (κ , λ , and γ) can be used as a first guess in error attenuation:

$$F_r = K_r d^\lambda V^\gamma f^\kappa \quad (17)$$

K_r , λ , γ and, κ are to be calibrated for each tool-workpiece, tool-work material combinations, process types, tool-wear condition, workpiece hardness, tool geometry, and speed. For the presented results, the applied voltage to the actuator is estimated first from both Eq. (17) and Figure 8. The subsequent applied voltage values are then obtained from the neurofuzzy

output voltage factor of Figure 11 based on the resulted error and the rate of error values. Actuator data for the obtained final results are given in Table 1. Using few numbers of PWM cycles per force period can cause unfavorable switching dynamic excitation by the actuator to tool post. The results in Figure 12 are the outcome of five PWM cycles, twenty PWM cycles per force period produce more favorable results but more than twenty have little effect. Cutting force fluctuations have a component that is proportional to the undeformed chip thickness and a component due to the rate of penetration called a plowing effect. For comparison, the results of increasing β in equation (16) by ten folds of the selected datum of 1% damping ratio for first mode and 5% for the second mode indicated a significant reduction in tool tip normalized error. In addition to the effectiveness of the Neurofuzzy algorithm both damping and NPWM (N_{PWM}) have contributed to the reduction in normalized error as shown in Figure 12. The results of Figure 12 points out that high damping alone do not ensure the minimum error attenuation. Sample results showing the effectiveness of the developed Neurofuzzy algorithm for error attenuation at different dampings are shown in Figure 12.

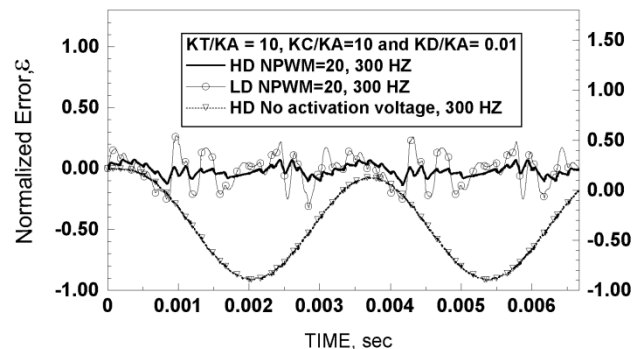


Figure 12: Normalized tool tip error versus time for neurofuzzy controller at high damping (HD), low damping (LD) and different NPWM's

The negative normalized error in Figures 12-13 indicates outward tool tip retraction away from workpiece axis. Tool bit to actuator stiffness ratio (KT/KA) has an importance in terms of force availability for tool tip error elimination and accurate displacement sensing as shown in Figure 8. Stiffness ratios greater than ten produce identical displacements between the tool tip and tool carrier main body. Taking into consideration the geometrical factors, significant deviation starts when stiffness ratio (KT/KA) drops below one. The importance of such parameter depends on the design configuration of the tool post and the acceptable range for the tool error.

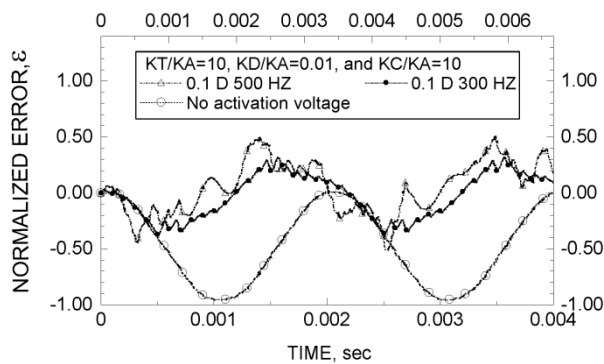


Fig. 13 Comparison between normalized tool tip errors at different frequencies for no delay (ND) and with 10% time delay (0.1 D)

of tool tip errors. Results are compared for two frequencies as shown in Figure 13.

VII. CONCLUSIONS

The application of neurofuzzy techniques to control a smart tool post has been presented. An adaptive learning algorithm for the neurofuzzy controller has been developed. The advantages of the proposed schemes are that an accurate model to describe the dynamics of the tool post is no longer needed, and the choice of learning parameters for the controller is not critical. With the proposed method, the controller can be easily designed and expanded. Designing against cutting tool error in turning machines using smart material reduce industrial waste, save money and, improve design flexibility for future tool generations. In this work critical frequencies of two modeling schemes are compared for a smart tool post under open and short circuit conditions. The results indicate significant differences between lumped mass modeling and FEM solution at low diaphragm to actuator stiffness ratio (KD/KA) and high tool carrier to actuator stiffness (KC/KA). This range of stiffness ratio has been investigated to ensure better error attenuation in smart material actuation for such applications. The work outcome can identify the stiffness range of lumped mass modeling that has more realistic representation of the dynamic response control. Also, suggest the use of high tool bit to tool carrier stiffness for better actuation capability and smaller tool tip error. Generated results suggest a reasonable number of at least twenty PWM segments should be used in representing the force cycle to reduce switching dynamic transient effects. The developed methodology in generating voltage activation factor to modify the static voltage-force-displacement value proved absolute effectiveness in error attenuation. The developed neurofuzzy algorithm to predict the voltage activation factor is based on both normalized error and rate of change in error and proved an ultimate success independent of forcing frequency. The neurofuzzy algorithm for voltage activation has contributed in reducing the too post error.

REFERENCES RÉFÉRENCES REFERENCIAS

1. Abboud, N. N., Wojcik, G. L., Vaughan, D. K., Mould, J., Powell, D. J., and, Nikodym, L., 1998 "Finite Element Modeling for Ultrasonic Transonic Transducers," Proceedings SPIE Int. Symposium on Medical Imaging, San Diego, Feb 21-27, pp. 1-24.
2. Allik, H., and, Hughes, T. J. R.: Finite element method for piezoelectric vibration. International Journal for Numerical Methods in Engineering, 2, pp. 151-157 (1970).
3. Bathe, K. J., 1982 "Finite Element Procedures in Engineering Analysis" Prentice-Hall Inc, pp.511-537.
4. Frankpitt, B. A., 1995 "Model of the Dynamics of a Lathe Toolpost that Incorporates Active Vibration Suppression. Institute for System Research," University of Maryland at College Park.
5. Frankpitt, B. A., 1995 "Model of the Dynamics of a Lathe Toolpost that Incorporates Active Vibration Suppression," Institute for System Research, University of Maryland at College Park.
6. Gopalakrishnan, V., Fedewa, D., Mehrabi, M. G., Kota, S., and, Orlandea, N., 2002, "Design of Reconfigurable Machine Tools," ASME J. Manuf. Sci. Eng., Technical Briefs, 124, pp. 483-485.
7. Harms, A., Denkena, B., and, Lhermet, N., 2004, "Tool adaptor for Active Vibration Control in Turning Operations," Actuator, 9th International Conference on New Actuators, Bremen, Germany. Pages 694 - 697.
8. Jang, J. J., Chuen-Tsai Sun, C. T., Mizutani, E., 1996, "Neuro-Fuzzy and Soft Computing: A Computational Approach to Learning and Machine Intelligence," Prentice Hall.
9. Kalinski, K J., Galewski, M A. 2011, "Chatter vibration surveillance by the optimal-linear spindle speed control", Mechanical Systems and Signal Processing, 25, pp 383-399
10. Lerch, R., 1990 "Simulation of piezoelectric devices by two and three dimensional finite elements," IEEE Transactions on Ultrasonics, Ferroelectrics, and Frequency Control, 37(3), pp. 233-247.
11. Lin, J. and Chao, W.S., 2009 "Vibration Suppression Control of Beam-cart System with Piezoelectric Transducers by Decomposed Parallel Adaptive Neuro-fuzzy Control," Journal of Vibration and Control, December, vol. 15 no. 12 1885-1906
12. Moon, Y., and, Kota, S., 2002, "Design of Reconfigurable Machine Tools", ASME J. Manuf. Sci. Eng., Technical Briefs, 124, Nov., pp. 480-483.
13. Park, G.a , Bement, M.T.a , Hartman, D.A.b , Smith, R.E.c , Farrar, C.R., 2007, "The use of active materials for machining processes: A review", International Journal of Machine Tools and Manufacture, Volume 47, Issue 15, pp 2189-2206

14. Piefort, V., 2001 "Finite Element Modeling of Piezoelectric Active Structures" Ph.D. Thesis, ULB, Active Structures Laboratory - Department of Mechanical Engineering and Robotics.
15. Radecki, P.P., Farinholt, K.M., Park, G. , Bement, M.T., 2010, " Vibration suppression in cutting tools using a collocated piezoelectric sensor/actuator with an adaptive control algorithm", ASME Journal of Vibration and Acoustics, 132, 5, pp 0510021-0510028
16. Rashid, M.K., .2005, "Simulation Study on the Improvements of Machining Accuracy by Using Smart Materials" Robotics and Computer-Integrated Manufacturing, Elsevier Science, Volume 21, Issue 3, June, Pages 249-257
17. Rashid, M.K., and, Shihab, K.I., 2006 "Intelligent Design of Cutting Tools Using Smart Material" International Journal of Mechanics and Materials in Design, Volume 3, Number 1, March, Pages 17-27 .
18. Roark R. J. and Young W. C., 1975 "Formulas for Stress and Strain" 5th edn, New York: McGraw-Hill, p 337 (table 24-1j).
19. Tzou, H. S., 1991 "Design of a piezoelectric exciter/actuator for micro-displacement control: theory and experiment," Precision Engineering, Vol. 13, No. 2, pp.104-110.
20. Zienkiewicz, O. C., and, Taylor, R. L., 2000a "The Finite Element Method" Fifth edition Vol.1: The Basis. Butterworth-Heinemann.
21. Zienkiewicz, O. C., and, Taylor, R. L., 2000b "The Finite Element Method" Fifth edition Vol.2: Solid Mechanics. Butterworth-Heinemann, pp. 423-424.